New Measurement of $K_L \rightarrow \pi^0 e^+ e^- \gamma$

Elliott Cheu and Yeun Jeun Kim

May 5, 2006

Abstract

We report on a new measurement of the BR($K_L \rightarrow \pi^o e^+ e^- \gamma$). This analysis includes data from both the 1997 and 1997 E799-II runs. We reconstruct 131 events over a background of 18, which results in BR($K_L \rightarrow \pi^o e^+ e^- \gamma$) = $(2.12 \pm 0.20 \pm 0.13) \times 10^{-8}$.

1 Introduction

The decay $K_L \rightarrow \pi^o e^+ e^- \gamma$ is interesting for two main reasons. First, it can be used as a check of chiral perturbation theories [1]. Second, this decay can be used to determine the CP conserving component to $K_L \rightarrow \pi^o e^+ e^-$. The only other measurement of this decay mode comes from the 1997 KTeV run [2], though there was also a search done at KEK [3].

This analysis is a combined analysis of the 1997 and 1999 data for $K_L \rightarrow \pi^o e^+ e^- \gamma$. We treat each of the data sets separately, then calculate the weighted average for the two data sets. Our analysis follows closely the work described in [2] and [4], but we have reoptimized the cuts. In addition, we have made a few improvements to the analysis, namely improved rejection of $K_L \rightarrow \pi^o \pi^o$ and $K_L \rightarrow \pi^o \pi^o \pi^o$ events, better simulation of the fusion χ^2 variable and production of a sizeable sample of Monte Carlo events. Unfortunately, we do not find a huge improvement in the signal to noise over the previous measurement. However, this result does have almost a factor of 2.5 improvement in the total number of candidates.

The data used is the output of the EEGGG subset of the 2E-NCLUS crunch. This data is contained on the NQND01-06 tapes.

2 Event Reconstruction and Analysis

Our analysis starts by requiring that the 2ENCLUS L3 tag has been satisfied. The requirements imposed by the EEGGG crunch are listed in Table 1. Each event is then required to have exactly two oppositely signed tracks and five hardware clusters. The two tracks are required to point to two of the clusters and form a decay vertex. Three different combinations of the remaining three photons can be formed. We choose the combination that reconstructs closest to the π^o mass. Because of its improved resolution, the neutral decay distance determined from the π^o is used to determine the masses of the $e^+ e^- \gamma$ and $e^+ e^- \gamma\gamma\gamma$ combinations.

To reduce the background from charged pions, the E/p for each of the tracks was required to be between 0.95 and 1.05. We required the decay vertex to reconstruct between 98 and 157 meters

and the transverse momentum squared to be less than 0.003 (GeV/c)^2. To select the π^o decay, we rejected $\gamma\gamma$ combinations with masses more than 5 MeV/c^2 away from the nominal π^o mass.

A number of cuts are made to improve the trigger simulation agreement between the Monte Carlo and the data. These include VV' verification, bad spill rejection, minimum cluster energy, minimum track separation at DC1, a cut on E_{CA} and a requirement on the distance between a cluster and either of the beam holes. All of theses cuts are also listed in Table 1.

3 Background Reduction

In this analysis we consider backgrounds from $K_L \to \pi^o\pi^o$ and $K_L \to \pi^o\pi^o\pi^o$ events, where one of the π^o's decays via a Dalitz decay ($\pi^o \to e^+e^-\gamma$). The $2\pi^o$ decays are more readily removed since the invariant mass of the $e^+e^-\gamma$ and $\gamma\gamma$ combinations usually reconstructs to the mass of a π^o. There will be an irriducible background from $2\pi^o$ events when the final state is misreconstructed, or if one or more of the final particles is lost to be replaced by an accidental particle. The $3\pi^o$ events are more difficult to remove because we cannot use the same mass constraint as in the $2\pi^o$ case. However, kinematic variables and cluster shape cuts help to reduce the background to a manageable level.

The vast majority of the background from $K_L \to \pi^o\pi^o$ can be removed by just cutting out events that have a mass near the π^o mass in the $m_{e^+e^-\gamma}$ distribution. However, in a non-negligible fraction of the events, the best m_{π^o} combination will not be the correct combination. In the previous analysis, a cut was made in the m_{π^o} versus $m_{e^+e^-\gamma}$ distribution for the second and third best combinations. To better take advantage of the correlations between the m_{π^o} and $m_{e^+e^-\gamma}$ distributions for the second and third best combinations, a neural net was used where the four input variables were the m_{π^o} and $m_{e^+e^-\gamma}$ for the second and third combinations. The neural net used sixteen hidden nodes and was tuned on a small sample of $2\pi^o$ and $\pi^o e^+e^-\gamma$ Monte Carlo. The neural net produces a function that weights each of the four variables to produce a single output value. This value is shown in Figure 1 for $2\pi^o$ and $\pi^o e^+e^-\gamma$ events. As can be seen, there is good separation between the signal and background samples.

In our analysis we require $NN > 0.95$ which is 88% efficient for $K_L \to \pi^o e^+e^-\gamma$ events. The position of the cut was determined by calculating the significance

$$S = \frac{N_{sig}}{\sqrt{N_{sig} + N_{bkg}}}$$

which is also shown in Figure 1. There is a broad peak in the significance plot with the maxium around 0.95.

The effect of this cut on the signal Monte Carlo can be seen in Figure 2. The cut on the neural net variable removes a cluster of events near the π^o mass in both the $e^+e^-\gamma$ and $\gamma\gamma$ distributions for the second best combination. For the third best combination, the effect of the cut is to remove a broad swath in the $\gamma\gamma$ variable.

After making the neural net cut, the remaining $2\pi^o$ events consist mainly of events with the correct π^o combination. These events will exhibit a peak in the $m_{e^+e^-\gamma}$ mass as shown in Figure 3 for $2\pi^o$ Monte Carlo. To remove this background we require the $e^+e^-\gamma$ mass to be less than 0.110 GeV/c^2 or greater than 0.155 GeV/c^2. The $2\pi^o$ events which fall outside of this cut will contribute

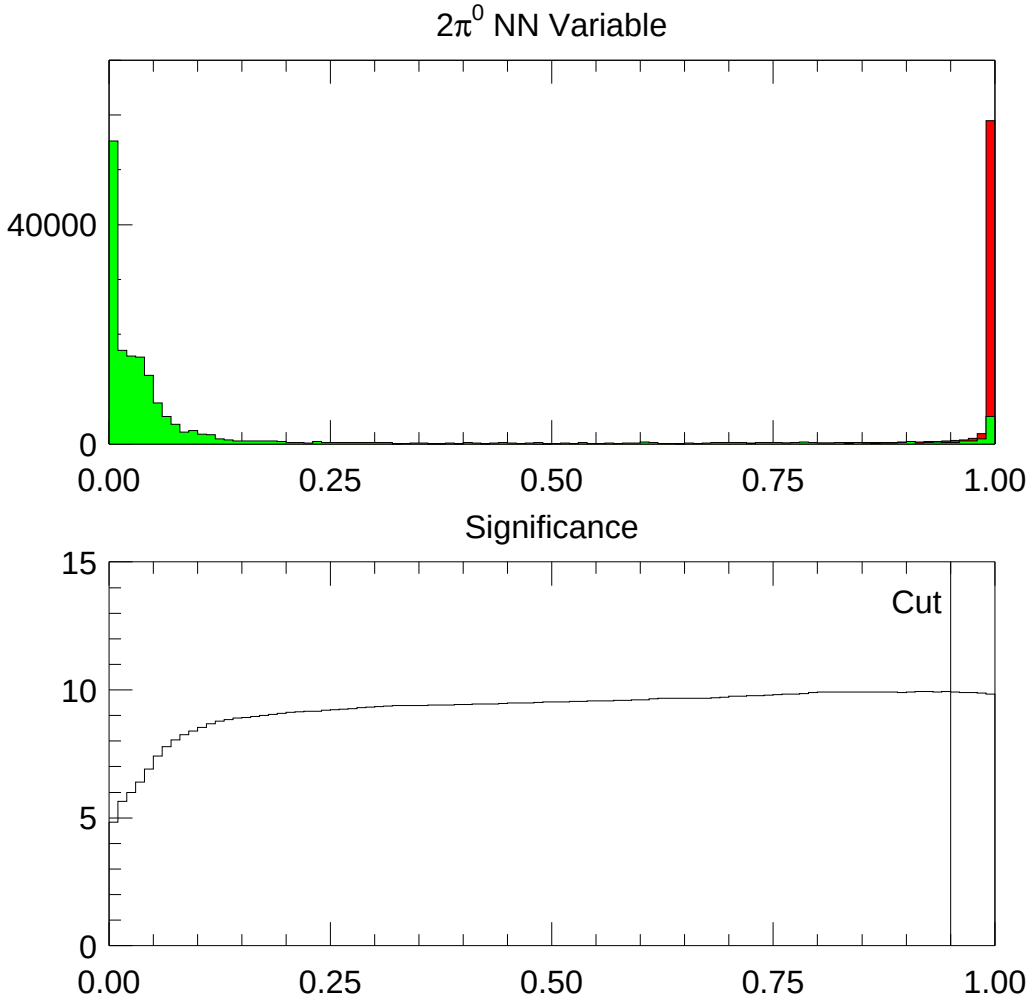

Figure 1: a) The $2\pi^o$ neural net variable for $2\pi^o$ (green) and $\pi^o e^+ e^- \gamma$ (red) Monte Carlo events. Events with a good π^o mass in the best $e^+ e^- \gamma$ combination have been removed. b) The significance (see text) as a function of the cut value. The line indicates the position of our cut.

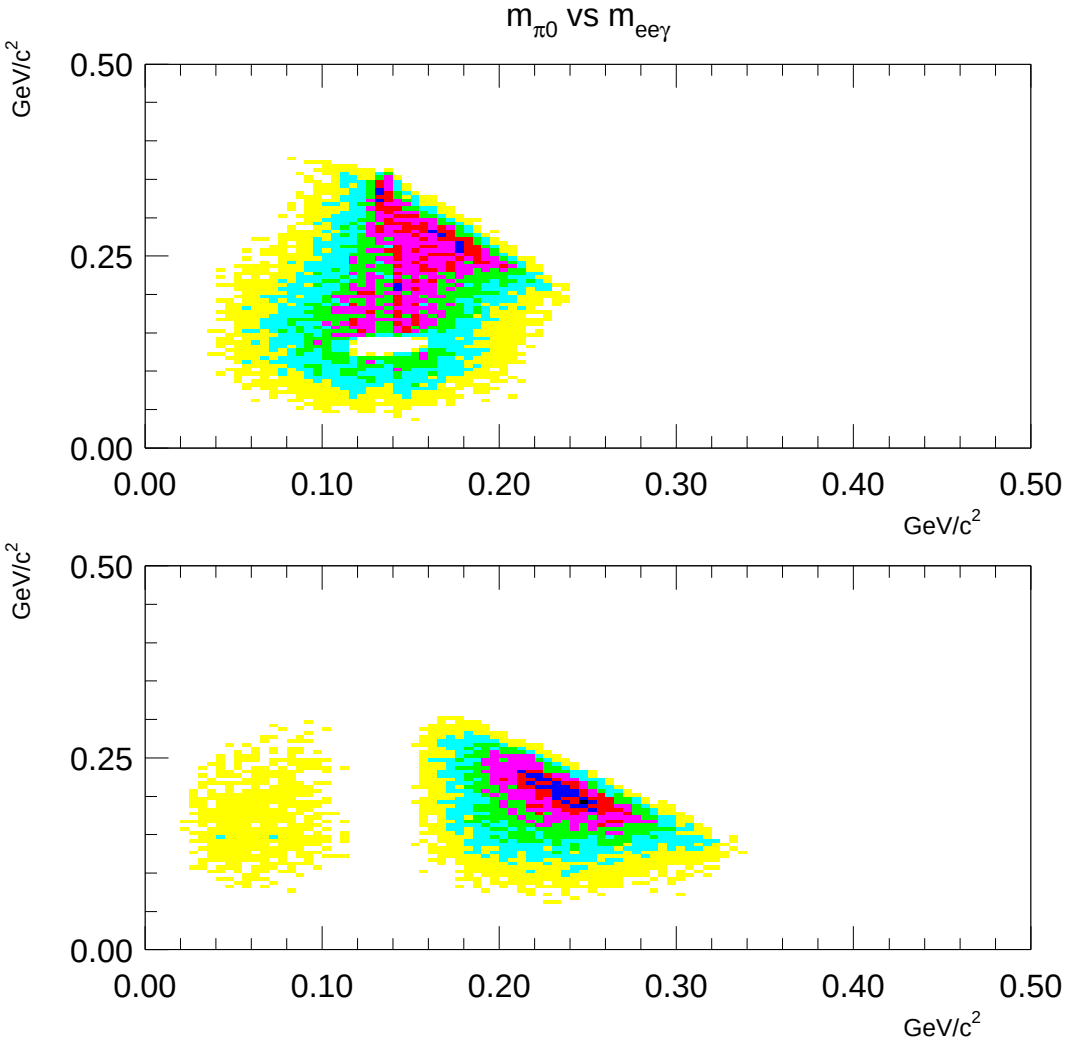

Figure 2: The distribution of the $m_{\gamma\gamma}$ versus $m_{e^+e^-\gamma}$ for $K_L \to \pi^o e^+ e^- \gamma$ Monte Carlo events after applying the $2\pi^o$ neural net cut. The top plot shows the second best combination while the bottom plot shows the third best combination.

to the irreducible background. Our cut and the cut used in the previous analysis are shown on this plot. From our perspective the previously used cut seems to be a little too loose.

Backgrounds from $K_L \to \pi^o\pi^o\pi^o$ come from two broad classes of events: events with missing photons and those with fused photons. For events with missing photons, we use the photon vetoes to significantly reduce the amount of background. We require the maximum energy in any ring counter to be less than 0.05 GeV. We also require that the energy in the spectrometer antis (and CsI anti) to be below 0.1 GeV. Plots of these variables can be seen in Figure 4.

Events with missing photons will also have a large value of pp0kin since the kaon momentum will be misreconstructed. The invariant mass of the three photons also is different for $3\pi^o$ events and signal because of the two extra two photons in the $3\pi^o$ decays. In the previous analysis, a two-dimensional cut was made in the pp0kin versus $m_{\gamma\gamma\gamma}$ plane. This cut is shown in Figure 5. As can be seen, at high values of $m_{\gamma\gamma\gamma}$, this cut significantly cuts into the $2\pi^o$ events without improving the signal-to-noise significantly. In our analysis we employ the following fourth-order polynomial.

$$\text{pp0kin}_{max} = A + B*(m_{\gamma\gamma\gamma} - x_0) + C*(m_{\gamma\gamma\gamma} - x_0)^2 + D*(m_{\gamma\gamma\gamma} - x_0)^3 + E*(m_{\gamma\gamma\gamma} - x_0)^4$$

where A = 3.9, B=-112.8, C=1256.6, D=-5861.8, E=10506.0 and $x_0 = 8.326 \times 10^{-2}$. This cut is superimposed upon the pp0kin versus $m_{\gamma\gamma\gamma}$ distribution in Figure 5.

To optimize this cut we varied the size of the normalization term, A. Figure 6 shows the efficiency of the signal and background as a function of the offset of the curve relative to the nominal position. An offset of zero maximizes the significance in this variable and retains about 90% of the signal.

The CsI simulation used in KTEVMC does not do a great job of describing the shape of the clusters in the data. In Figure 7 we compare the FUSE3x3 variable between data and Monte Carlo. The FUSE3x3 variable uses the 3x3 array of blocks around the seed block. The default fusion χ^2 variable uses a 5x5 array of blocks. We choose this variable, since it seems to be a bit more sensitive to fusions than the default 5x5 variable. As can be seen in the plot, the agreement between the data and Monte Carlo is not very good.

To achieve better agreement between the data and Monte Carlo, we have skimmed off showers from $K_L \to \pi^o\pi^o$ and $K_L \to \pi^+e^-\nu$ events to create a shower library from data events. During the Monte Carlo simulation, we chose an appropriate shower from this library and stored an array of energies for each cluster. The default shower simulation (using GEANT showers) was also done in the normal way. The new array of energies was written out along with the GEANT CsI information. This new array of energies was then used to calculate the fusion χ^2 for each cluster, while the default shower simulation was used to describe the reconstructed energies and positions of the clusters. To properly describe the fusion χ^2, full clustering of the data shower library array was done and the FUSE3x3 variable was calculated. As can be seen in Figure 7, the agreement between the data and Monte Carlo simulation improves significantly when using the data shower library. We make a cut at FUSE3X3 < 4 based upon the significance shown in Figure 6.

In the previous analysis of the 1997 data, a discrepancy between the data and MC was seen in the plot of the minimum distance between the projected position of an upstream track segment and a cluster in the CsI. A spike at low minimum distance is indicative of bremsstrahlung activity. This effect can be seen in Figure 8. Because of the discrepancy between the data and MC, it was hypothesized that there was a source of backgrounds not simulated by the $2\pi^0$ or $3\pi^0$. However, in our latest simulations of the $2\pi^0$ and $\pi^oe^+e^-\gamma$ decays, we do see a spike at low minimum

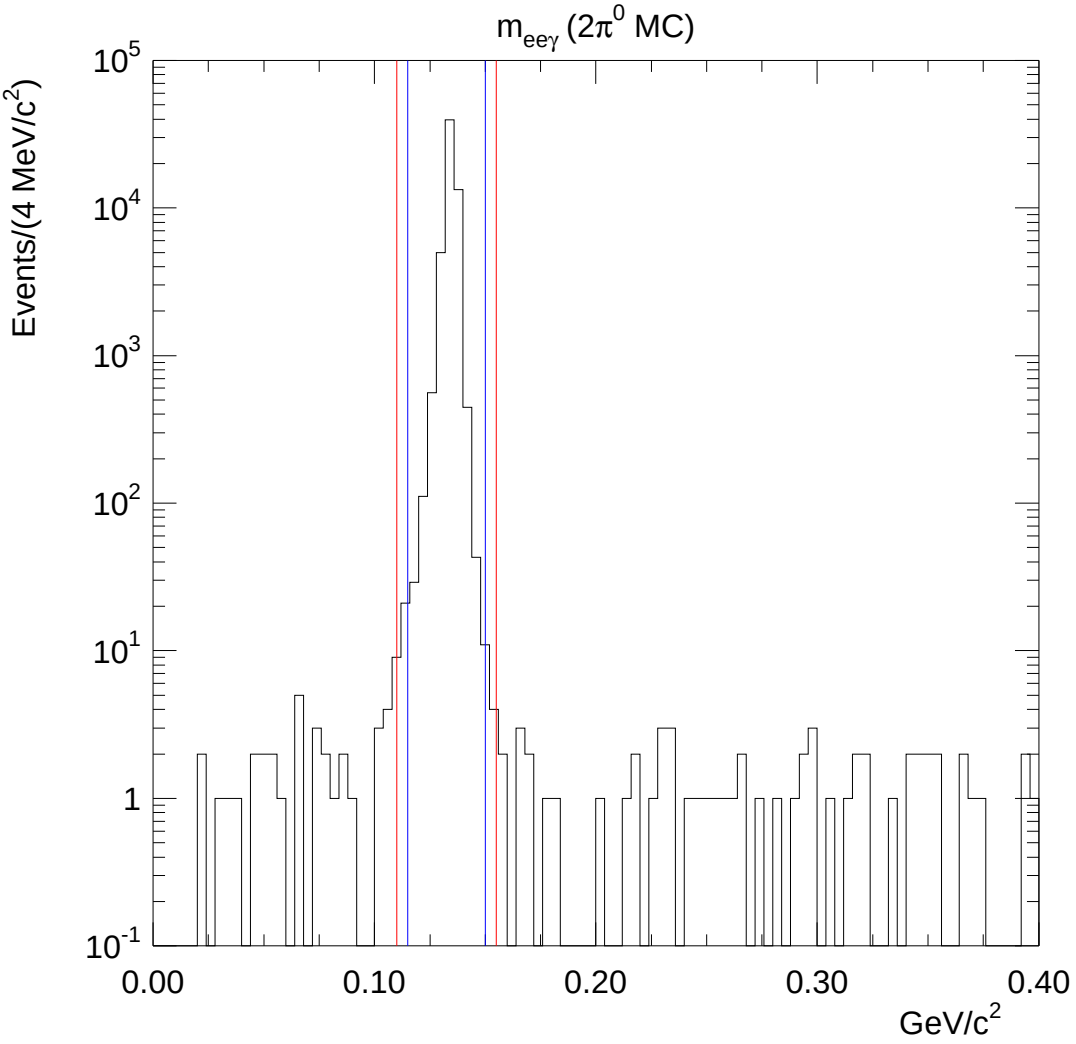

Figure 3: The $e^+e^-\gamma$ mass distribution for $2\pi^o$ Monte Carlo events. The cut from the previous analysis is indicated by the blue line, while our cut is shown in red.

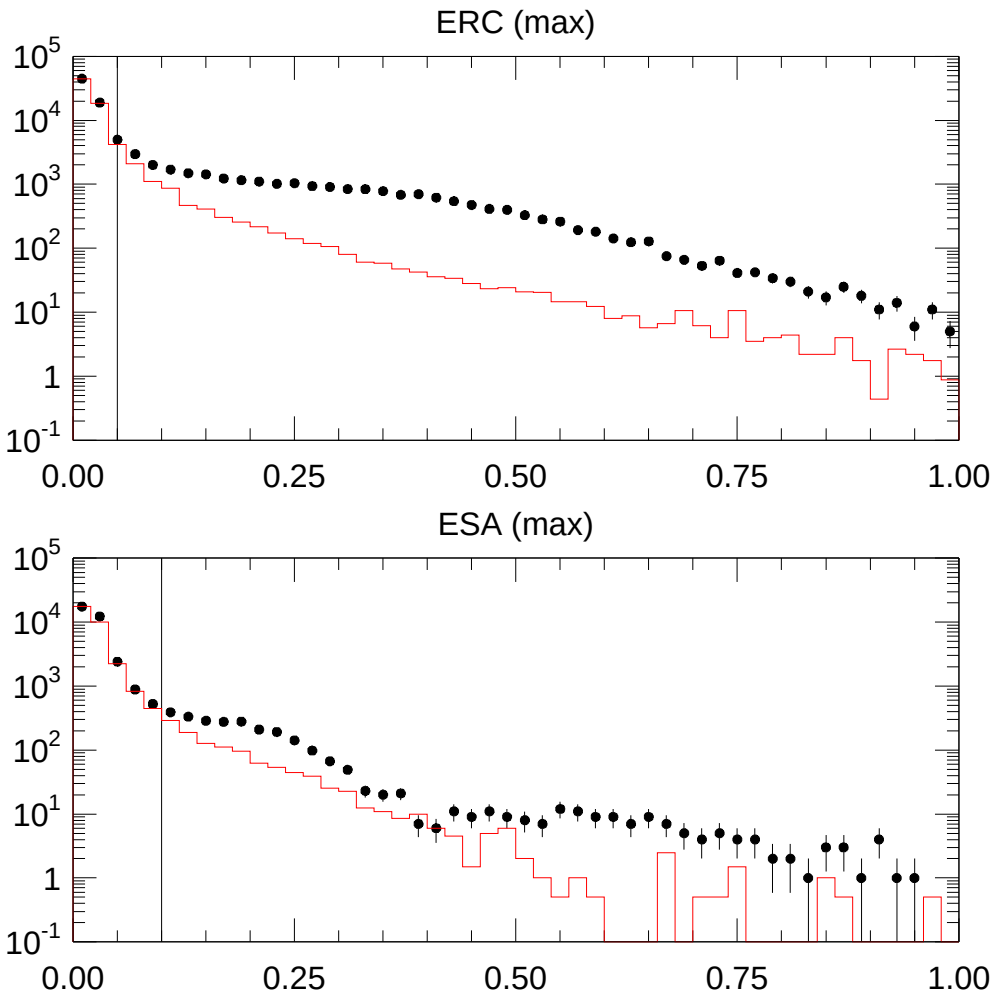

Figure 4: Maximum energy deposited in the RCs (top) and the SAs (bottom). The dots are the data and the red histogram is a Monte Carlo of $2\pi^o$ decays. The black line indicates the position of the cut.

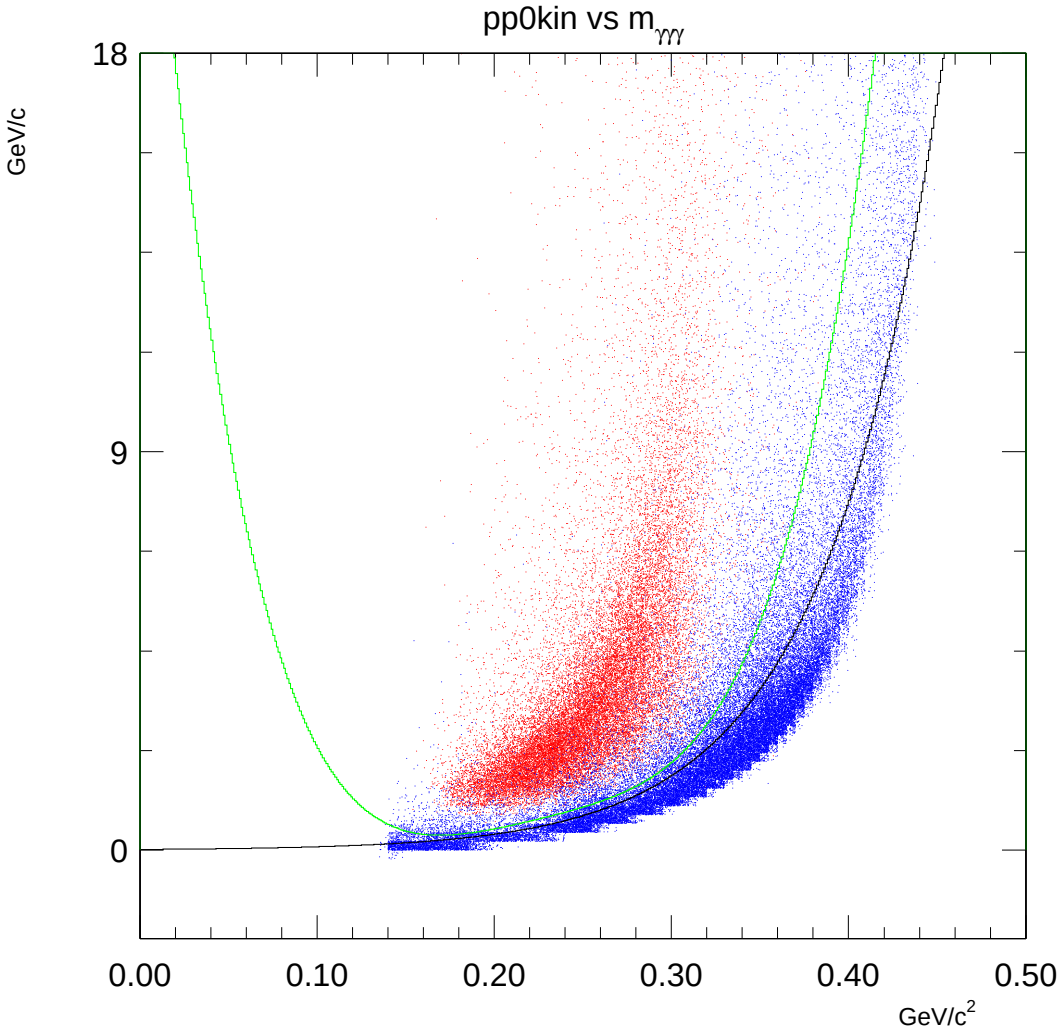

Figure 5: Distribution of pp0kin versus $m_{\gamma\gamma\gamma}$ for $K_L \rightarrow \pi^o\pi^o\pi^o$ (red) and $K_L \rightarrow \pi^o\pi^o$ (blue) Monte Carlo events. The black line represents the cut used in the previous 1997 analysis. The green line represents the cut used in this analysis. Events above the line are thrown out by the cut.

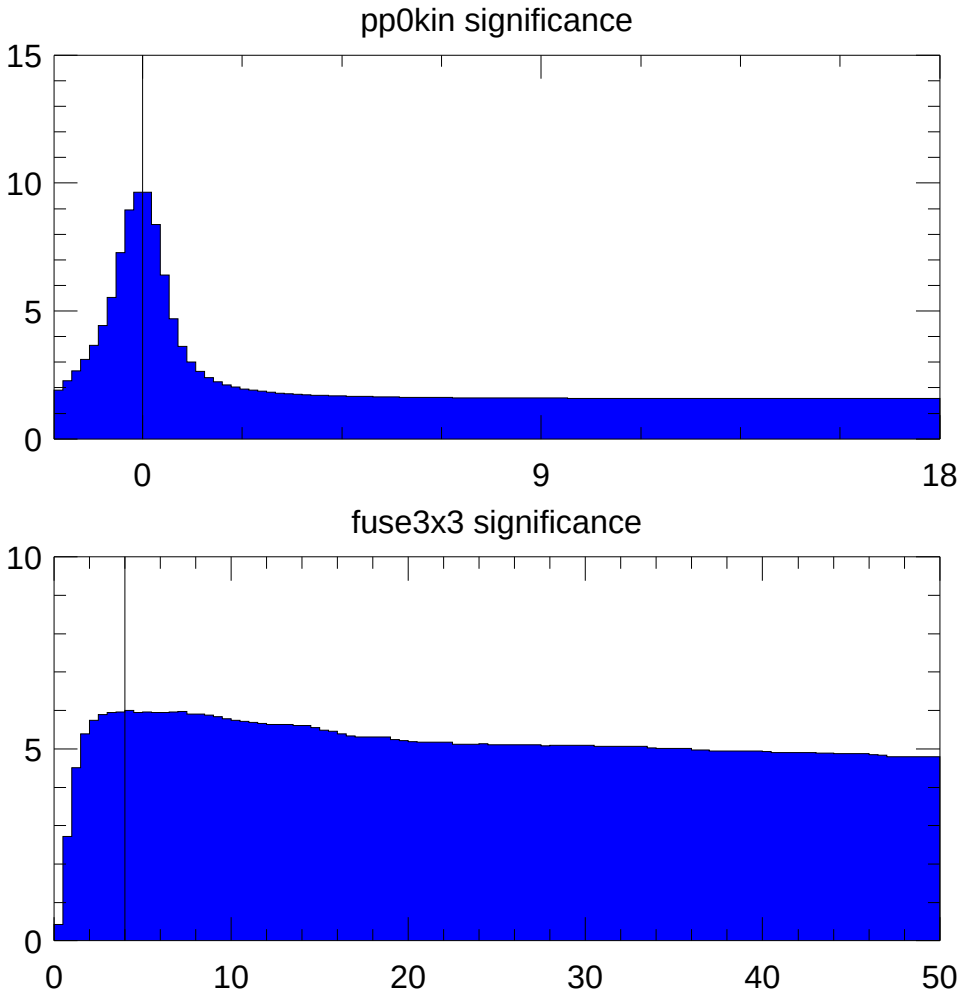

Figure 6: The top plot shows the significance of the cut for $\pi^o e^+ e^- \gamma$ events when varying the normalization term in the polynomial. The lower plot shows the significance as a function of the FUSE3X3 variable. The black lines indicate the position of the cuts.

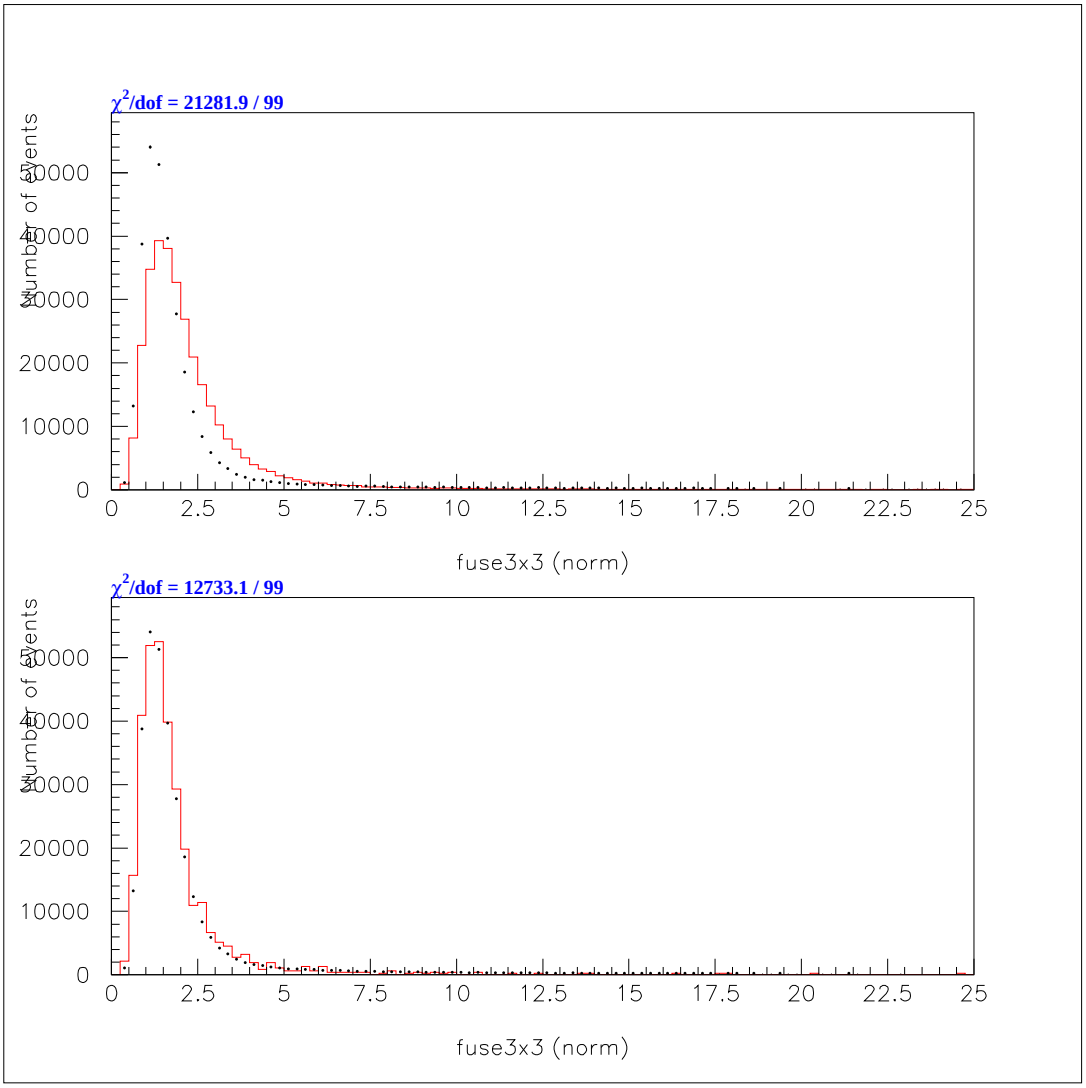

Figure 7: The FUSE3X3 variable for $K_L \rightarrow \pi^o\pi^o$ events. The crosses are the data and the red histogram represents the Monte Carlo simulation. The top plot shows the default Monte Carlo response, while the bottom plot shows the new Monte Carlo using data showers.

distance. Figure 9 shows the data/MC comparison for events satisfying all of the cuts except for the kaon mass requirement and the cut on the minimum track/cluster distance. As can be seen, the MC matches the data well, and also reproduces the spike seen at low cluster/track distance. In our Monte Carlo samples, we allowed at least one of the final state particles to be lost. So, a bremsstrahlung photon can substitute for one of the decay photons. In the default Monte Carlo, no lost photons are allowed. We surmise that the Monte Carlo used in the previous analysis used the default behavior.

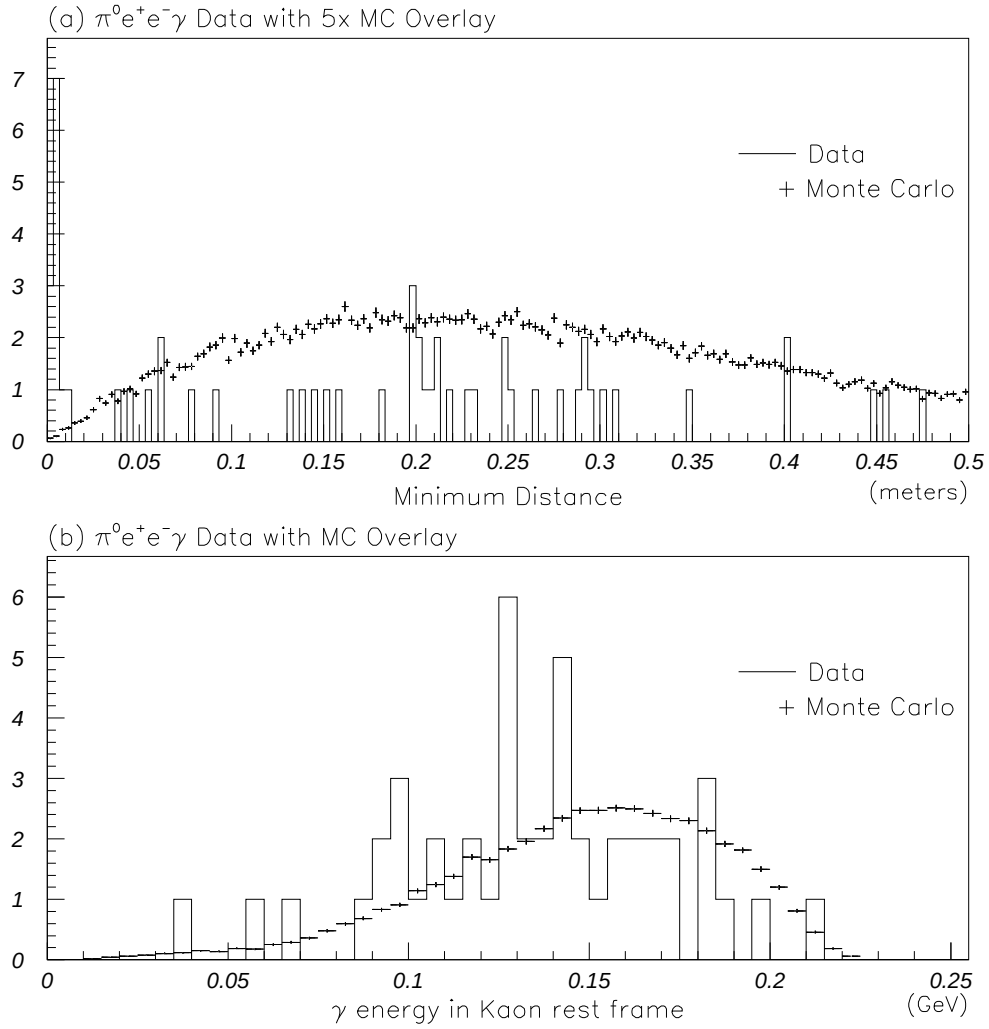

Figure 8: The minimum distance plot (top) and the γ energy distribution from the previous 1997 analysis.

After making the cut against $2\pi^o$ decays, we find the $e^+e^-\gamma\gamma\gamma$ mass distributions shown in Figure10. A clear peak at the kaon mass is seen. The background is well-described by the sum of

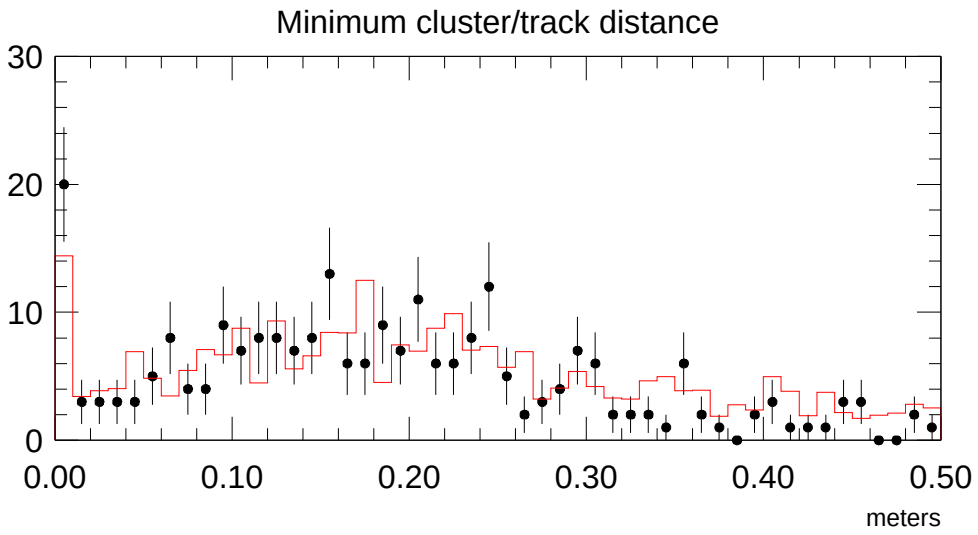

Figure 9: The minimum distance between clusters and the projected upstream track segments for all events satisfying all requirements except the kaon mass and minimum track distance cuts. The red histogram is the sum of signal plus background Monte Carlo, while the dots are the data. The mysterious spike at low minimum distance is well-represented by $3\pi^o$ Monte Carlo events.

the $2\pi^o$ and $3\pi^o$ background Monte Carlo samples.

The final cut applied is a requirement that the $m_{e^+e^-\gamma\gamma\gamma}$ mass fall between 0.490 and 0.505. Figure 11 shows the $e^+e^-\gamma$ mass for candidates which satisfy the kaon mass requirement. In the 1997 sample we find 46 events over a background of 4.4 ± 1.5 events. For the 1999 data set, our analysis obtains 86 events with an estimated background of 13.5 ± 2.6 events.

The $m_{e^+e^-\gamma}$ and $m_{e^+e^-\gamma\gamma\gamma}$ mass distributions for the combined 1997 and 1999 data sets are shown in Figure 12. Similar plots from our published PRL result are shown in Figure 13. While the plots are similar, there seems to be more background in the previous analysis. However, the signal-to-background ratio is about the same between the two analyses.

4 Branching Ratio Determination

The branching fraction is determined from the following expression:

$$BR = (N_{\pi^o e^+e^-\gamma}/N_{2\pi^o}) \times (\epsilon_{2\pi^o}/\epsilon_{\pi^o e^+e^-\gamma}) \times BR(K_L \to \pi^o\pi^o) \times BR(\pi^o \to e^+e^-\gamma) \times 2$$

$N_{\pi^o e^+e^-\gamma}$ represents the number of signal candidates, while $N_{2\pi^o}$ represents the number of normalization events. The number of $2\pi^o$ candidates is determined by removing the cut against $K_L \to \pi^o\pi^o$ events and counting the number of events in the kaon mass region from 0.490 to 0.510. In the above expresssion $\epsilon_{2\pi^o}$ and $\epsilon_{\pi^o e^+e^-\gamma}$ correspond to the reconstructed $K_L \to 2\pi^o$ and $K_L \to \pi^o e^+e^-\gamma$ acceptances, respectively. The factor of two occurs because there are two π^o per $K_L \to \pi^o\pi^o$ event. In the previous analysis, the value of BR($K_L \to \pi^o\pi^o$) used was

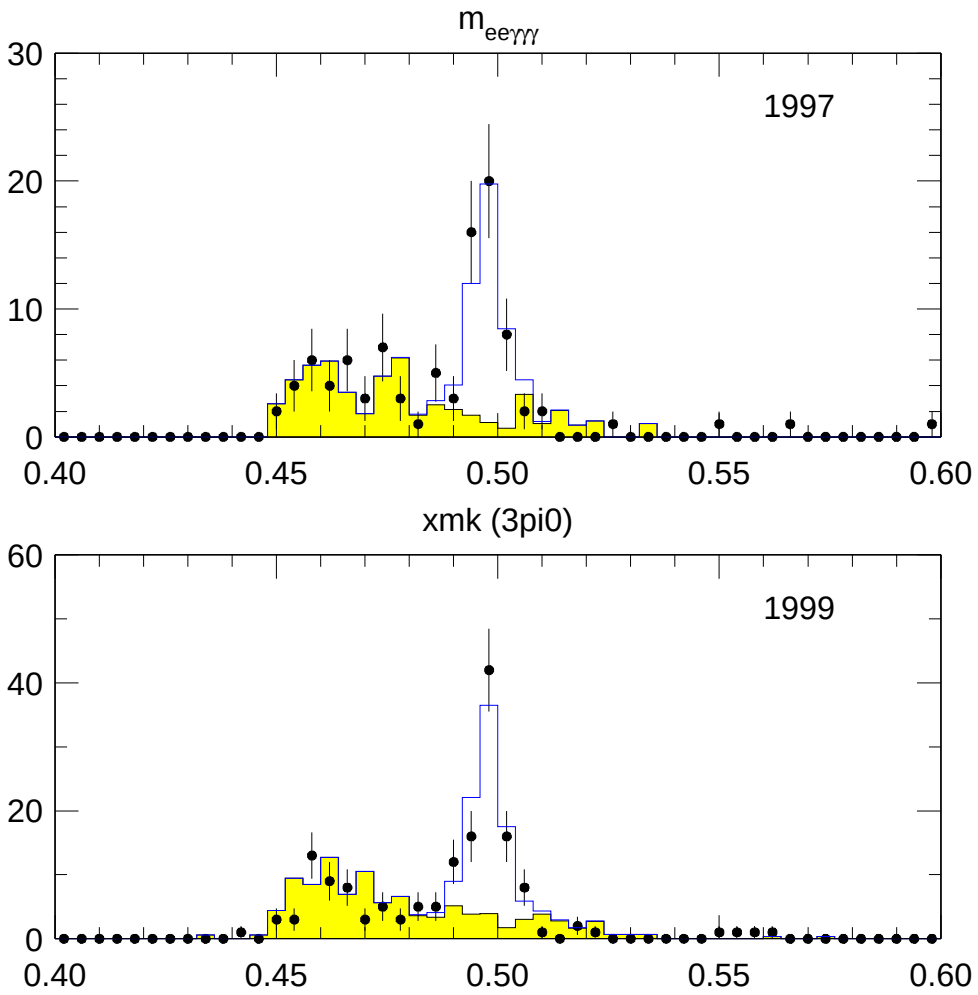

Figure 10: The reconstructed $e^+e^-\gamma\gamma\gamma$ mass for candidates passing all cuts but the cut on the kaon mass. The data are the dots while the yellow histogram is the Monte Carlo simulation of $2\pi^o$ and $3\pi^o$ events. The top plot shows the 1997 data and the bottom plot shows the 1999 data.

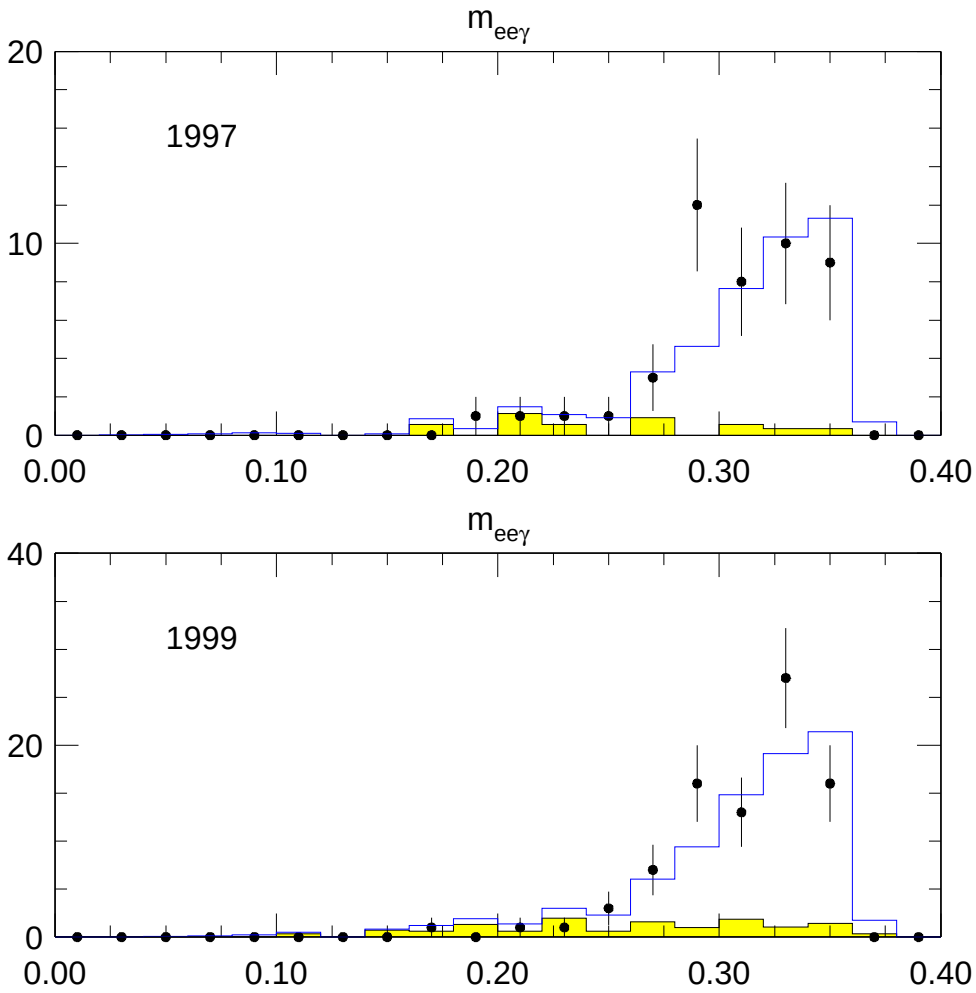

Figure 11: The $e^+e^-\gamma$ invariant mass for candidate $K_L \to \pi^o e^+ e^- \gamma$ events. The yellow histogram is the predicted background from $K_L \to \pi^o\pi^o$ and $K_L \to \pi^o\pi^o\pi^o$ events. The blue histogram shows the $K_L \to \pi^o e^+ e^- \gamma$ mass distribution for $a_V = -1.1$.

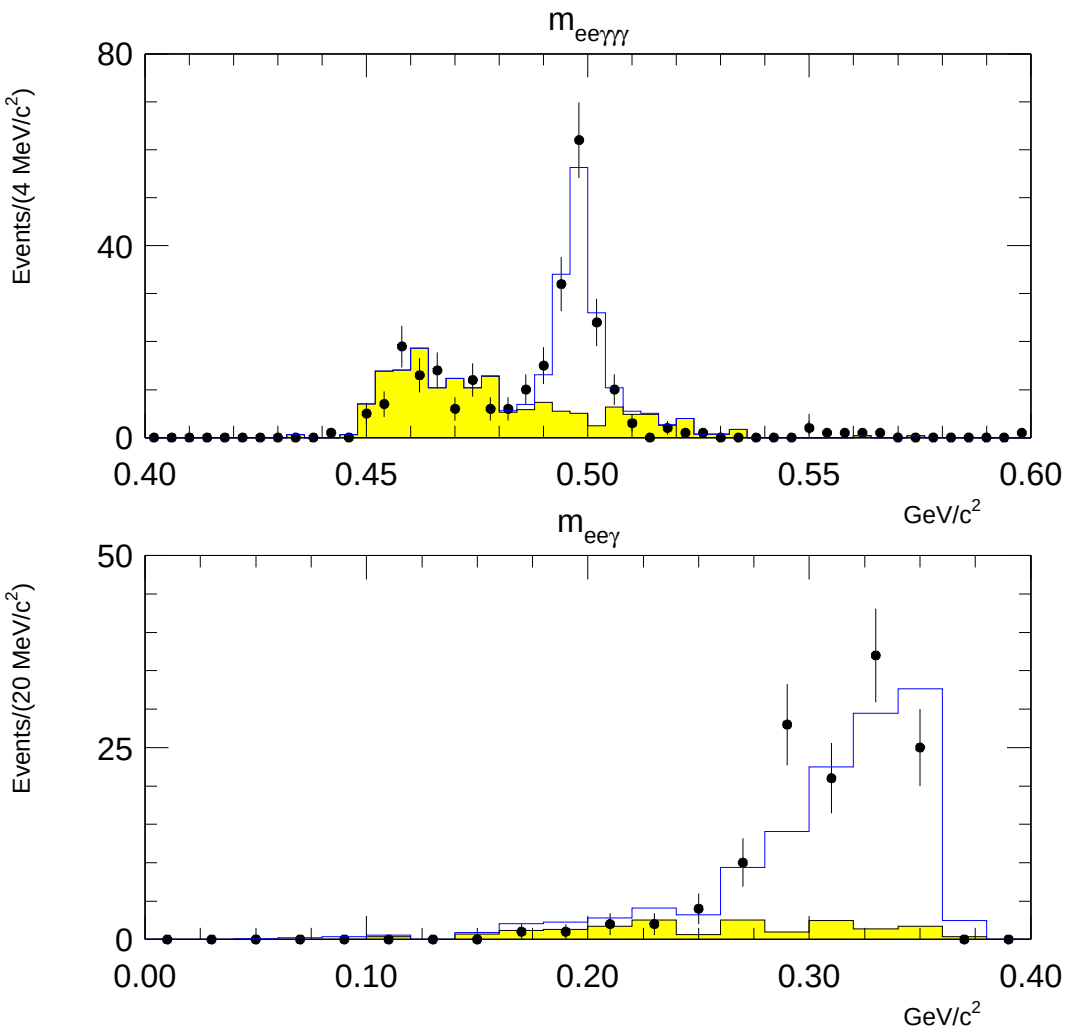

Figure 12: The reconstructed $e^+e^-\gamma\gamma\gamma$ mass (top) for the combined data sets for all events passing all cuts but the cut on the kaon mass. The data are the dots while the yellow histogram is the Monte Carlo simulation of $2\pi^o$ and $3\pi^o$ events. The bottom plot shows the $e^+e^-\gamma$ mass for the combined 1997 and 1999 data sets.

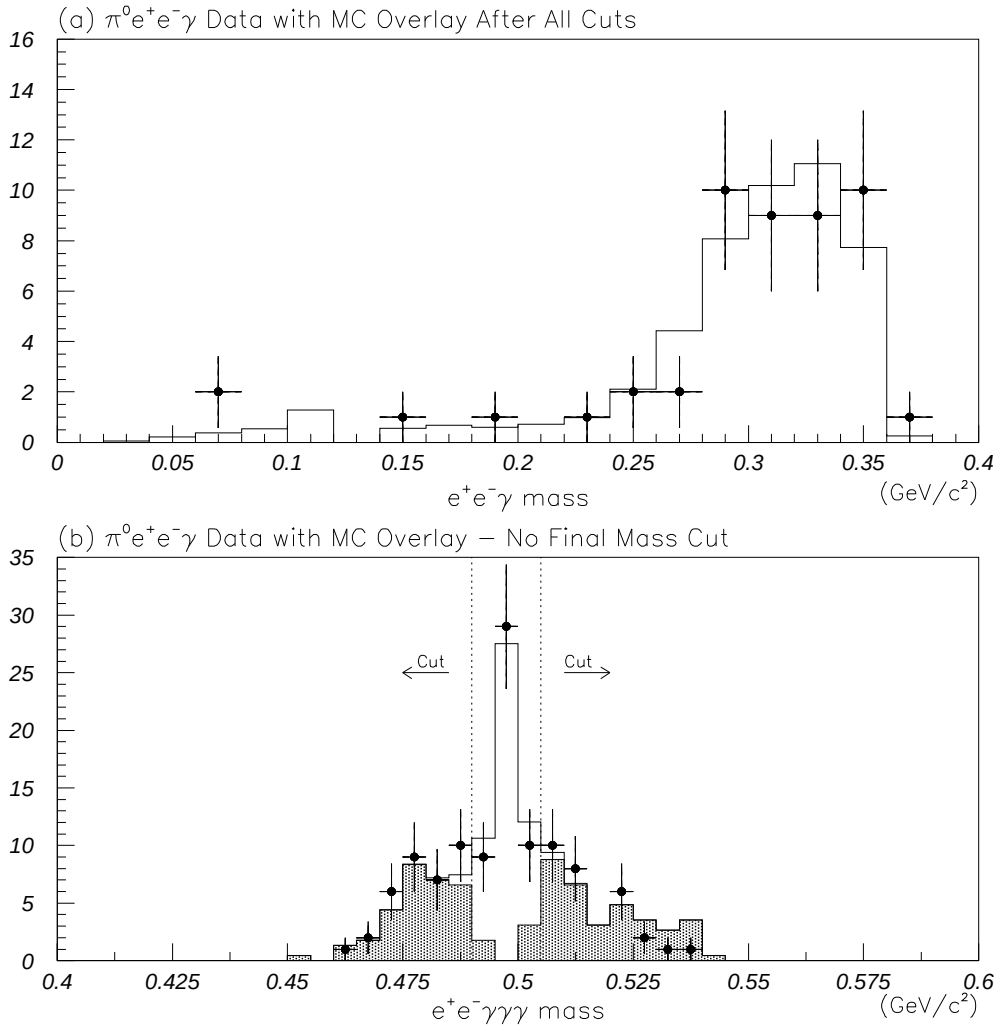

Figure 13: The reconstructed $e^+e^-\gamma$ mass (top) and $e^+e^-\gamma\gamma\gamma$ mass (bottom) from the published PRL result. The top plot is after all cuts, while the bottom plot is after all cuts except for the cut on the kaon mass.

$(9.36 \pm 0.2) \times 10^{-4}$. We are using the latest value of $(8.83 \pm 0.08) \times 10^{-4}$. To directly, compare the values one should scale down the previous value by 1.06. The value of BR($\pi^o \to e^+e^-\gamma$) used in both analyses is $(1.198 \pm 0.032) \times 10^{-2}$.

In G. Graham's analysis the value was BR($K_L \to \pi^o e^+ e^- \gamma$) $= (2.34 \pm 0.35 \pm 0.13) \times 10^{-8}$ for the 1997 data set. Rescaling by the ratio of the $2\pi^o$ branching ratios results in BR($K_L \to \pi^o e^+ e^- \gamma$) = $(2.21 \pm 0.33 \pm 0.12) \times 10^{-8}$.

The acceptance for $2\pi^o$ events is 0.48% in the 1997 data set and 0.57% in the 1999 data set. The difference between the two data sets arises from the decreased magnetic field used in 1999. The $\pi^o e^+ e^- \gamma$ acceptances are 0.58% and 0.74% for the 1997 and 1999 data sets, respectively. The acceptances for the three modes, $K_L \to \pi^o\pi^o$, $K_L \to \pi^o\pi^o\pi^o$ and $K_L \to \pi^o e^+ e^- \gamma$ all increased by about 20-30% between 1997 and 1999. Using the numbers above, we obtain:

$$\begin{aligned} \text{BR}(K_L \to \pi^o e^+ e^- \gamma) &= 1.98 \pm 0.31 \qquad \text{(1997)} \\ \text{BR}(K_L \to \pi^o e^+ e^- \gamma) &= 2.23 \pm 0.26 \qquad \text{(1999)} \end{aligned}$$

A plot of the results is shown in Figure 14. To check whether or not our result is consistent with G. Graham's result, we compared the statistics between the two analyses. We found that of the 45 events in the original sample, 12 are exclusive to that analysis. Of the 46 events in our final sample, 13 are exclusive to our 1997 analysis. Calculating the errors using the exclusive events, and adding the errors in quadrature, we find that the difference in the 1997 branching ratios is:

$$\text{BR(PRL)-BR(new)} = (0.23 \pm 0.23) \times 10^{-8},$$

where the error is the statistical. So, we conclude that the two results are compatible with each other. The values used to determine the branching ratio for the two results are shown in Table 2.

5 Systematics

We have broken down our systematics studies into two main classes: those that affect the background level and those that affect the determination of the acceptance. Since the backgrounds are significantly reduced by a few specific cuts, we concentrated on understanding the effects of those cuts.

Our main tool was to reweight the Monte Carlo events so that the data/MC comparison agreed. An example of this can be seen Figures 15 and 16. The first plot shows the $3\pi^o$ data/MC overlay before reweighting. The second shows the effect of the reweighting. In this particular case, the reweighting was done using a linear fit to the ratio, rather than the actual ratio. The fit was then normalized so that the average value across the plot was one. To determine a systematic error associated with a given variable, we calculated the branching ratio for the 1997 and 1999 data sets, separately. Then, we recalculated the background level after reweighting and took the difference as our systematic. For the $3\pi^o$ background, we considered the FUSE3x3 variable and the $3\pi^o$ pp0kin versus $m_{\gamma\gamma\gamma}$ cut. We also examined the $3\pi^o$ z and p distributions. Plots of these variables before and after reweighting can be seen in Figures 17-19.

The z distribution for the $3\pi^o$ Monte Carlo does not match particularly well the shape from the data as seen in Figure 17. One possibility for this difference could be due to the efficiency of the

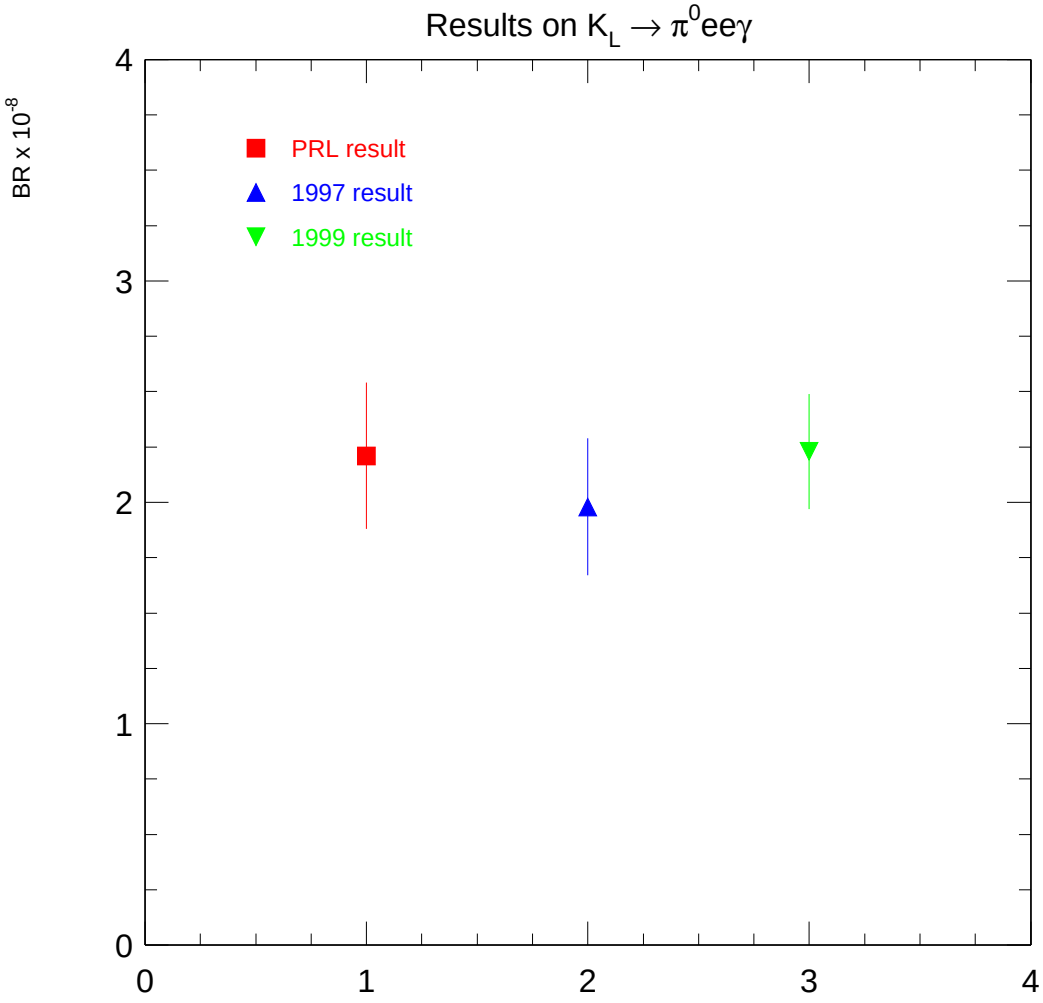

Figure 14: The results on the $K_L \to \pi^o e^+ e^- \gamma$ branching ratio.

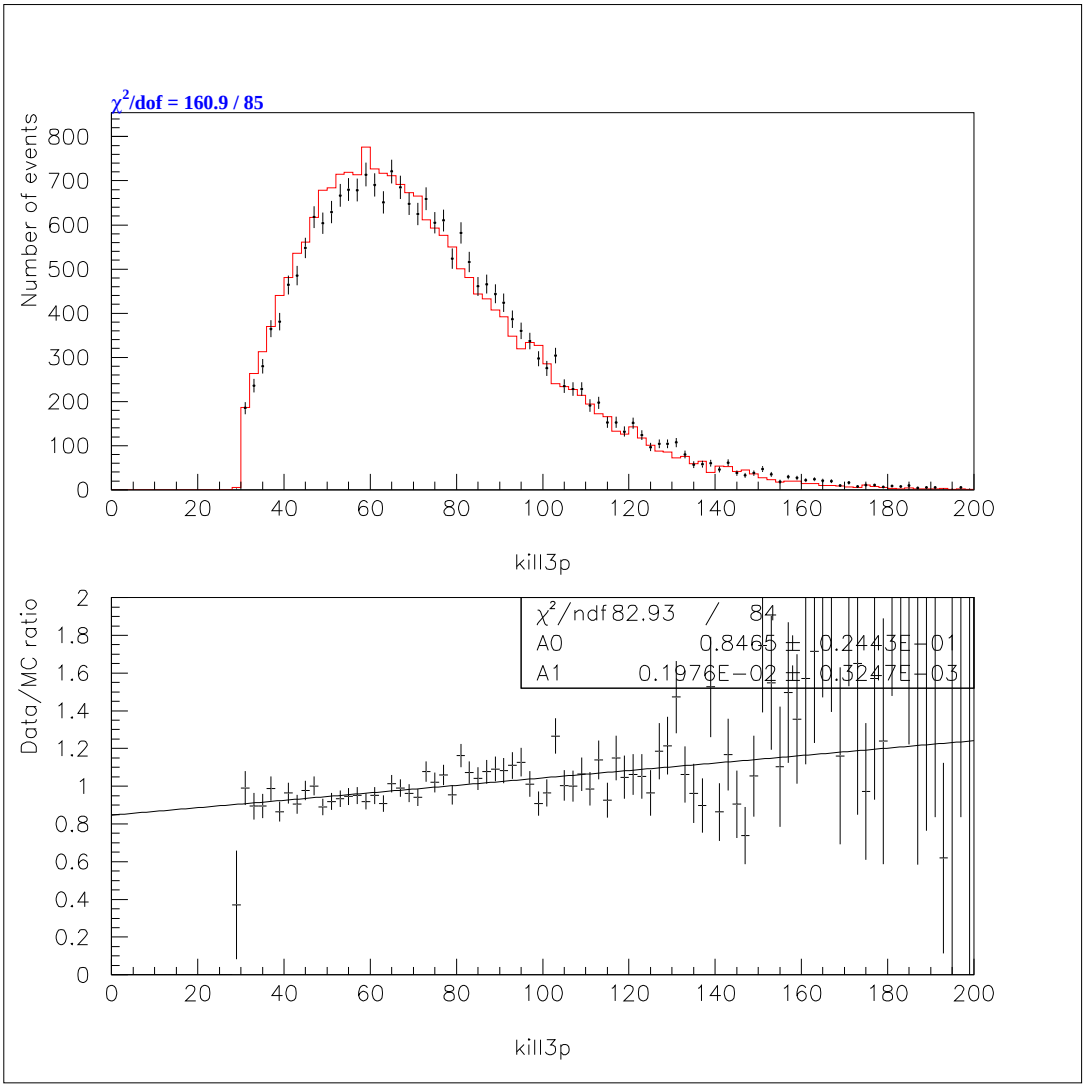

Figure 15: The kaon momentum distribution for $K_L \rightarrow \pi^o\pi^o\pi^o$ events. The crosses are the data while the red histogram represents the $3\pi^o$ Monte Carlo. These events have passed all of the cuts except for the cuts againts $3\pi^o$ events and the final kaon mass cut.

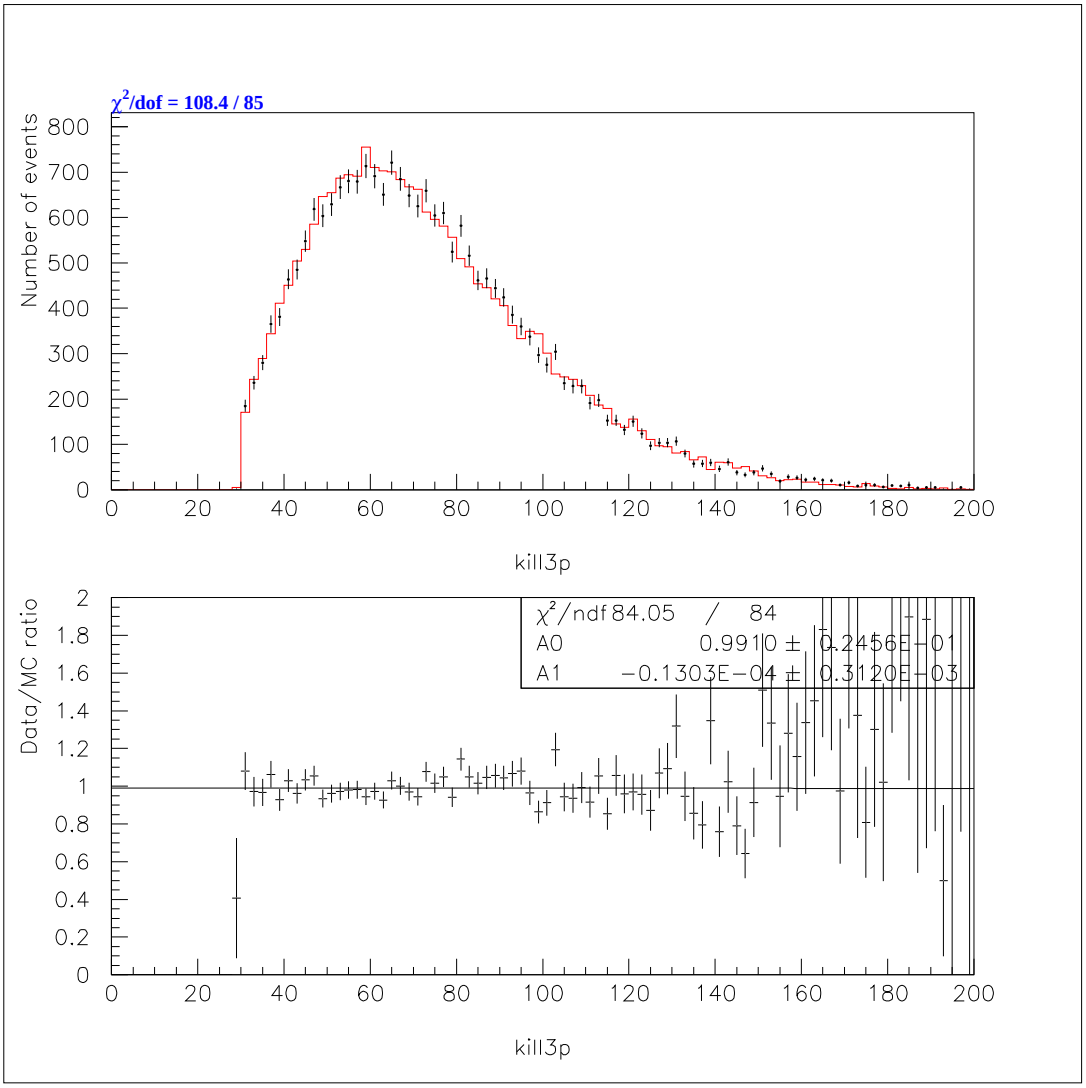

Figure 16: The kaon momentum distribution after reweighting. The data are the crosses and the Monte Carlo events the red histogram. The reweighting is not perfect because the reweighting function used the linear fit from the previous plot.

photon vetoes for the Monte Carlo versus the data. In events where photons are lost, the decay vertex is reconstructed downstream of the true decay vertex. Since the data/MC comparison for $2\pi^o$ decays looks good, we believe that the acceptance is well-modelled for events in which all of the particles are correctly reconstructed. After reweighting the Monte Carlo events, we find that the $3\pi^o$ background contribution changes by about one percent or so.

The other variable which helps to significantly reduce the $3\pi^o$ background is the cut against the pp0kin versus $m_{\gamma\gamma\gamma}$ variable. We parametrized this effect by looking at the offset of the normalization in the polynomial as shown in Figure 19. In this figure we included both the $3\pi^o$ and the $\pi^o e^+ e^- \gamma$ Monte Carlo before determining the data/MC ratio. After reweighting we found that the level of background changed by a very small amount, 0.3%.

For the $2\pi^o$ background, we considered the $2\pi^o$ neural net variable, and the $2\pi^o$ z and p distributions. The neural net variable can be seen in Figure 20. Surprisingly, the data and Monte Carlo match quite well. After reweighting the $2\pi^o$ Monte Carlo, we found that the background level increased by 0.3%.

The second class of systematics relates to the relative acceptance between the $K_L \to \pi^o\pi^o$ and $K_L \to \pi^o e^+ e^- \gamma$ events. Since we determine the $\pi^o e^+ e^- \gamma$ branching ratio by taking the ratio of the $\pi^o\pi^o$ to $\pi^o e^+ e^- \gamma$ acceptances, we are fairly immune to many systematic effects. To determine the systematic effects from various parameters, we reweighted both the $\pi^o\pi^o$ and $\pi^o e^+ e^- \gamma$ Monte Carlos by the ratio of data to Monte Carlo for the $\pi^o\pi^o$ events. In principle we should calculate the ratios separately for the $\pi^o\pi^o$ and $\pi^o e^+ e^- \gamma$ events, but we do not have the statistics for that. And, if we did have the statistics, we could just apply the correction and have essentially very little systematic effect to worry about. Here we considered parameters which affected the $\pi^o\pi^o$ acceptance the most. In particular, we examined the illumination of the CsI, the z distribution, and the p_T distribution. The $\pi^o\pi^o$ momentum distribution matched very well, and we do not calculate a systematic for it. This is shown in Figure 21.

By far the largest systematic comes from the dependence of the $K_L \to \pi^o e^+ e^- \gamma$ acceptance on the value of a_V. Figure 22 shows the χ^2 from fits of the $K_L \to \pi^o e^+ e^- \gamma$ Monte Carlo to the final $m_{e^+e^-\gamma}$ distribution. As can be seen, there is a minimum around $a_V = -1.1$. However, the one sigma error bar is from $a_V = -0.8$ to -1.40. Using this range as the uncertainty on the value of a_V, we find that the acceptance varies by about 7.6% for the 1997 data and 5.4% for the 1999 data. We can try to reduce this systematic by including the Y dalitz variable in our determination of a_V.

Table 3 lists each of the systematic effects considered and the relative shift in the branching ratio after reweighting. In addition to the studies that listed above, we also included systematics for the measured branching ratios of $K_L \to \pi^o\pi^o$ and $\pi^o \to e^+ e^- \gamma$. This systematic was added to the combined result rather than individually to the 1997 and 1999 result. The final systematic results from the limited statistics for the $2\pi^o$ and $3\pi^o$ Monte Carlo samples. For the 1997 and 1999 samples, we generated about three times the statistics of each data sample. For the $3\pi^o$ samples, we generated about two times the statistics. We considered generating more, but decided that given the time, disk space and effort, that it would not significantly improve our result since the result is statistically limited.

To obtain the final result, we took the weighted average of the 1997 and 1999 numbers. We weighted by the combined statistical and systematic error. Then, we added the common systematic errors, that due to the errors on the K_L and π^o branching ratios, to the final systematic error. The result is BR($K_L \to \pi^o e^+ e^- \gamma$) = $(2.12 \pm 0.20 \pm 0.13) \times 10^{-8}$.

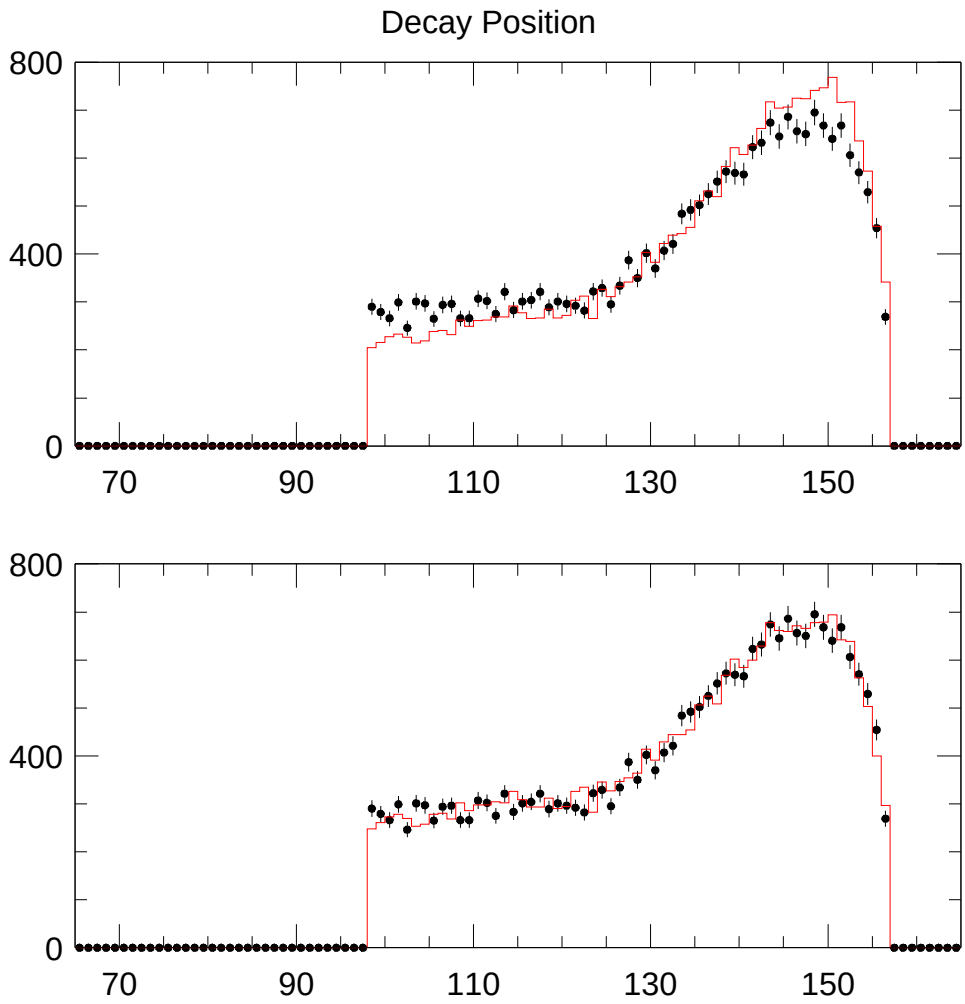

Figure 17: The z distribution for $3\pi^o$ events for data (crosses) and Monte Carlo (red). The top plot shows the events before reweighting while the lower plot shows the same events after reweighting. This plot shows the largest disagreement between the data and the Monte Carlo.

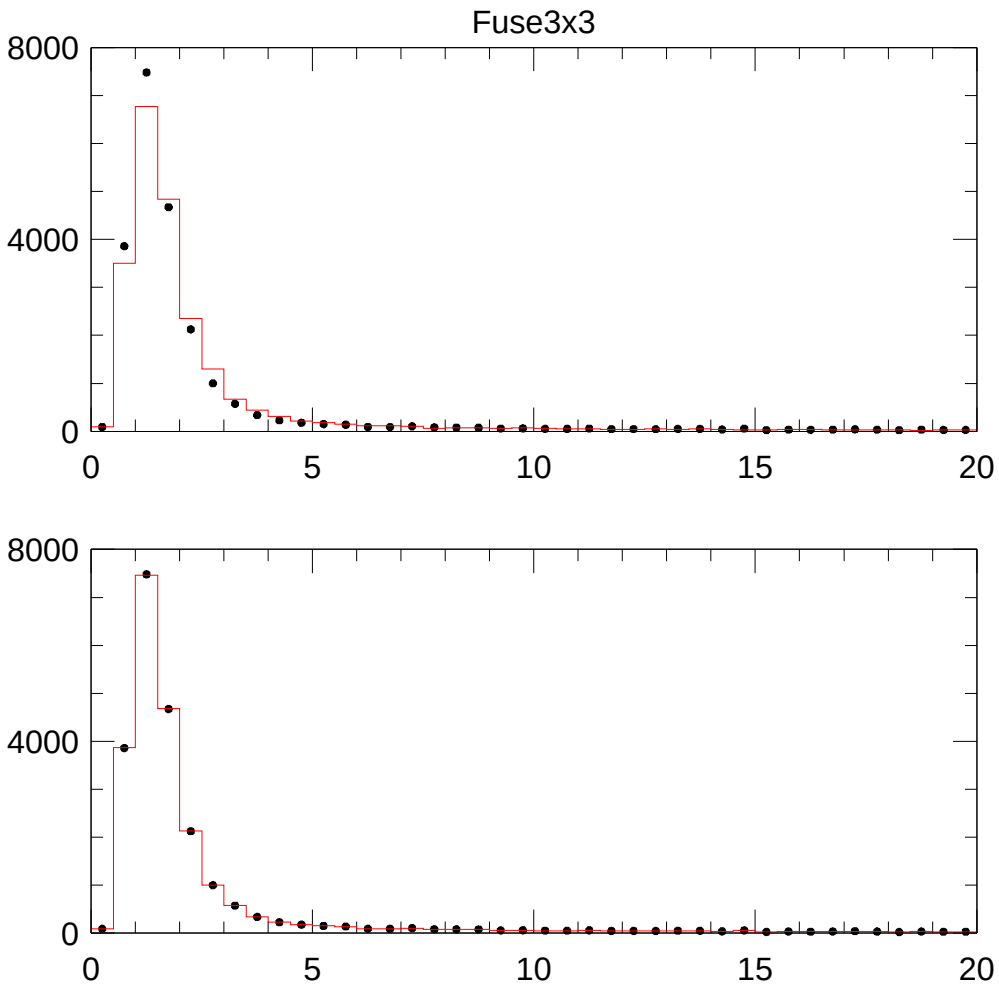

Figure 18: The FUSE3x3 variable.

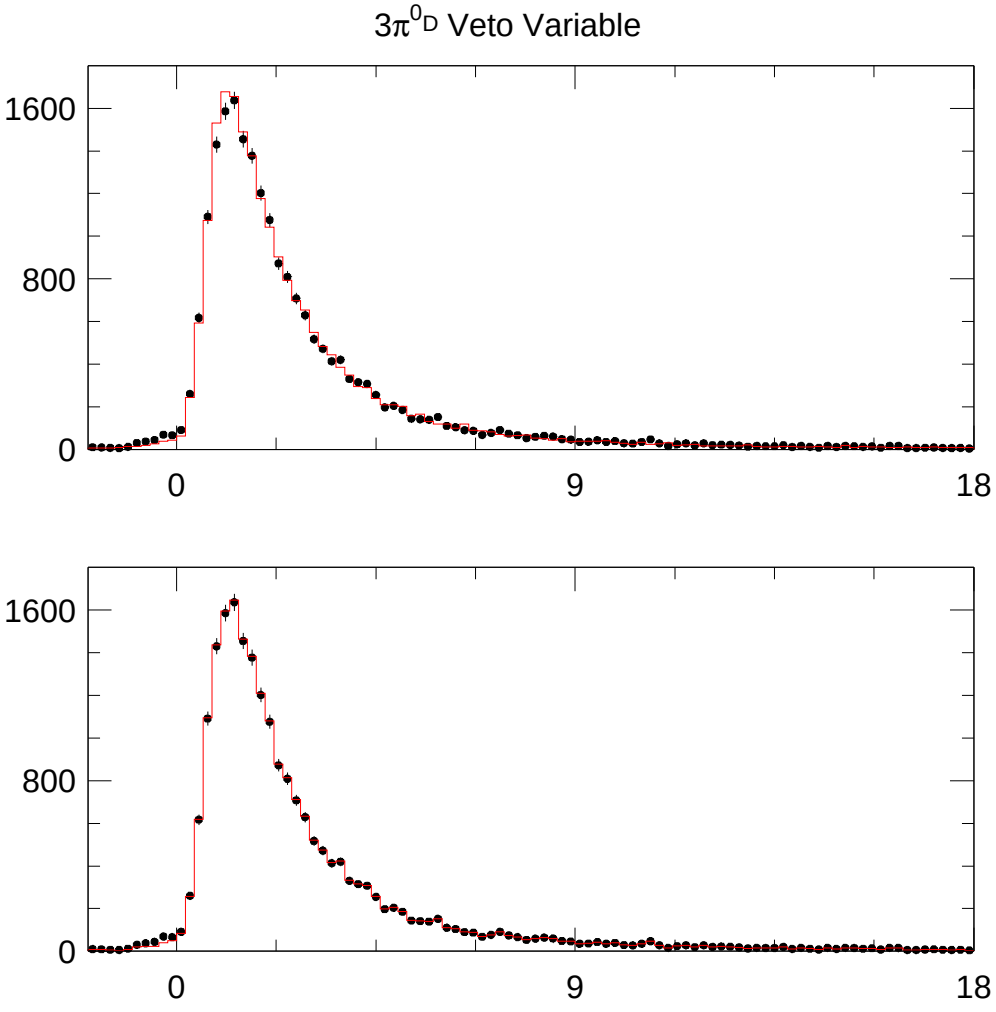

Figure 19: The $3\pi^o$ pp0kin/$m_{\gamma\gamma\gamma}$ variable for $3\pi^o$ data (crosses) and Monte Carlo (red). The top plot shows the distributions before reweighting. For this variable the reweighting was done after adding the $3\pi^o$ and the $\pi^o e^+ e^- \gamma$ Monte Carlos. This is because the $\pi^o e^+ e^- \gamma$ events populate the region right around the cut at zero.

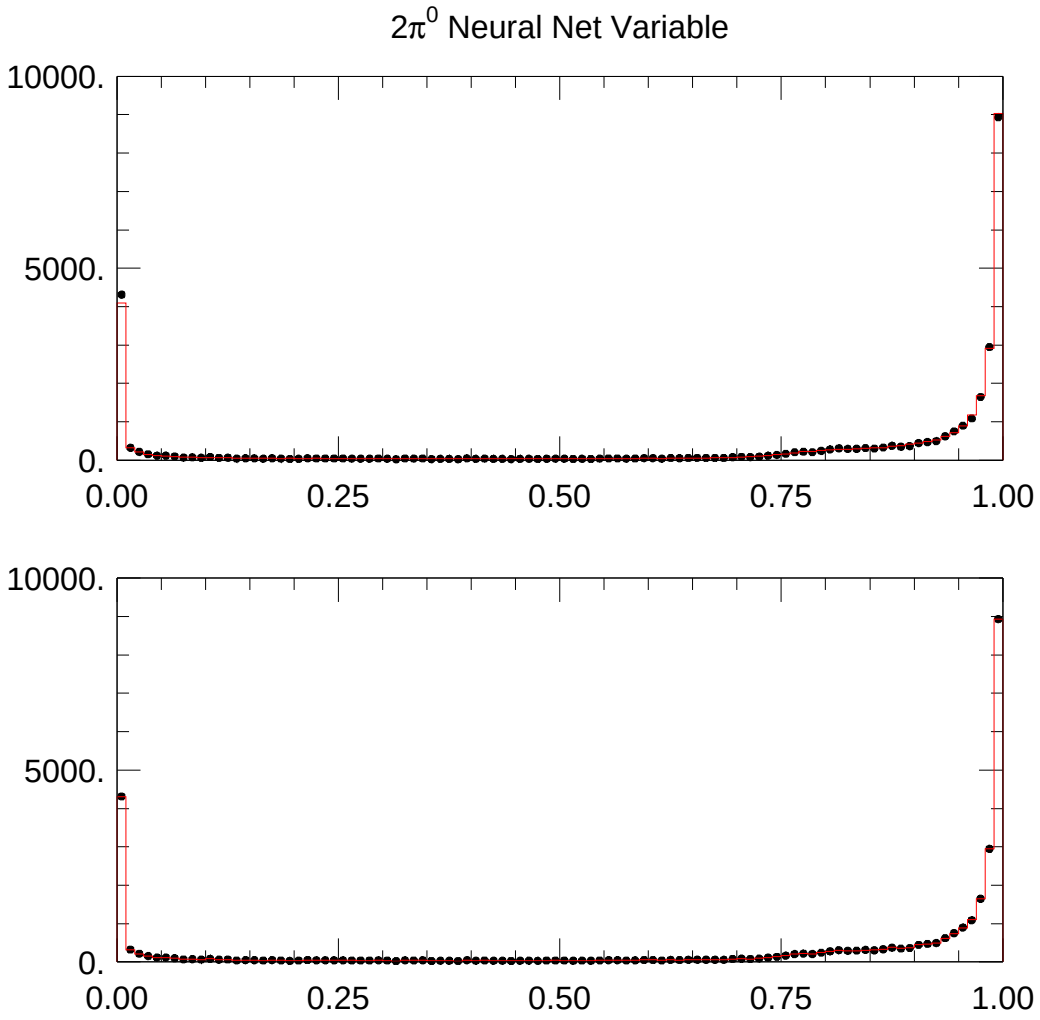

Figure 20: The $2\pi^o$ neural net variable for events passing all cuts except the neural net cut. The crosses are the data while the red histogram is the Monte Carlo.

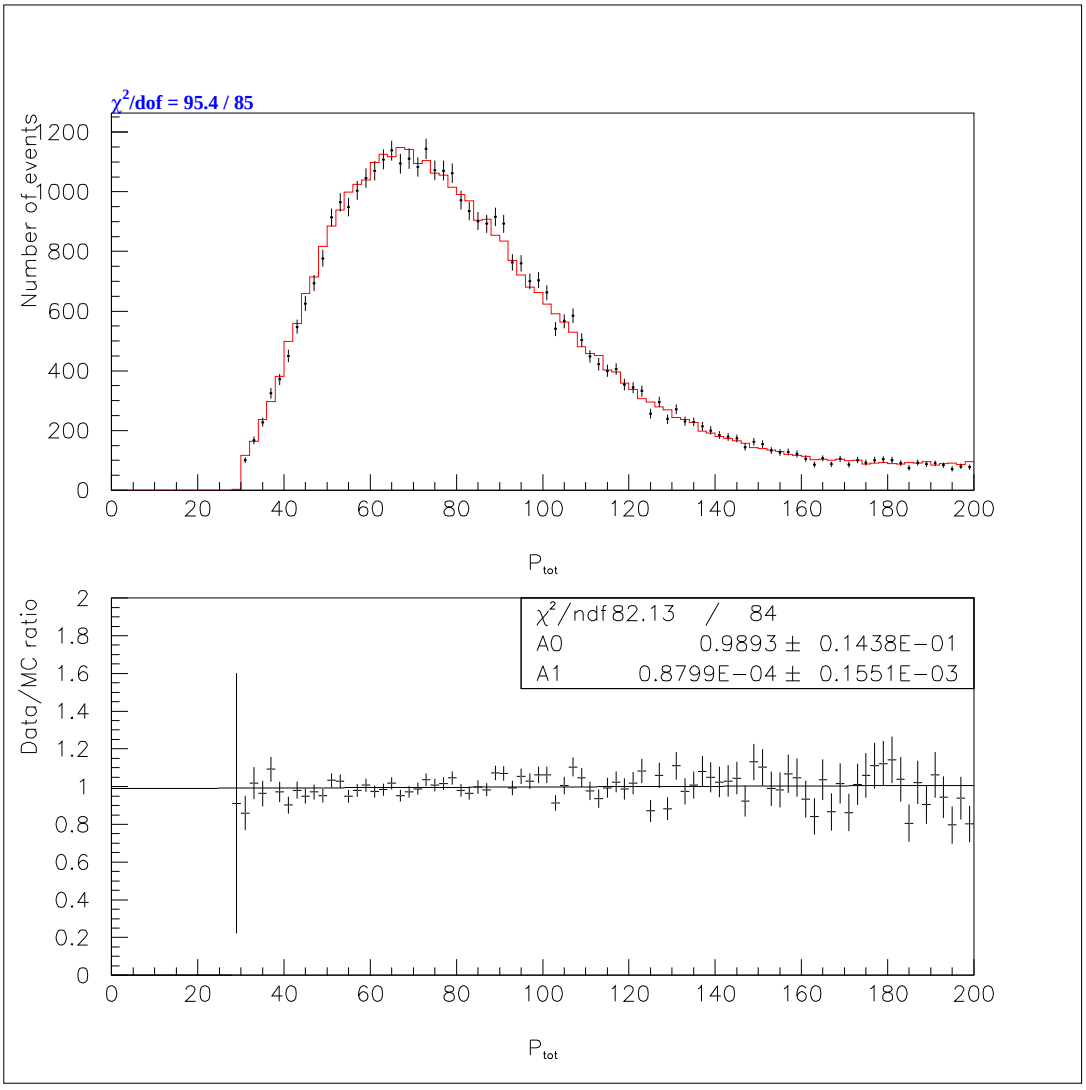

Figure 21: The comparison of the $\pi^o\pi^o$ total momentum.

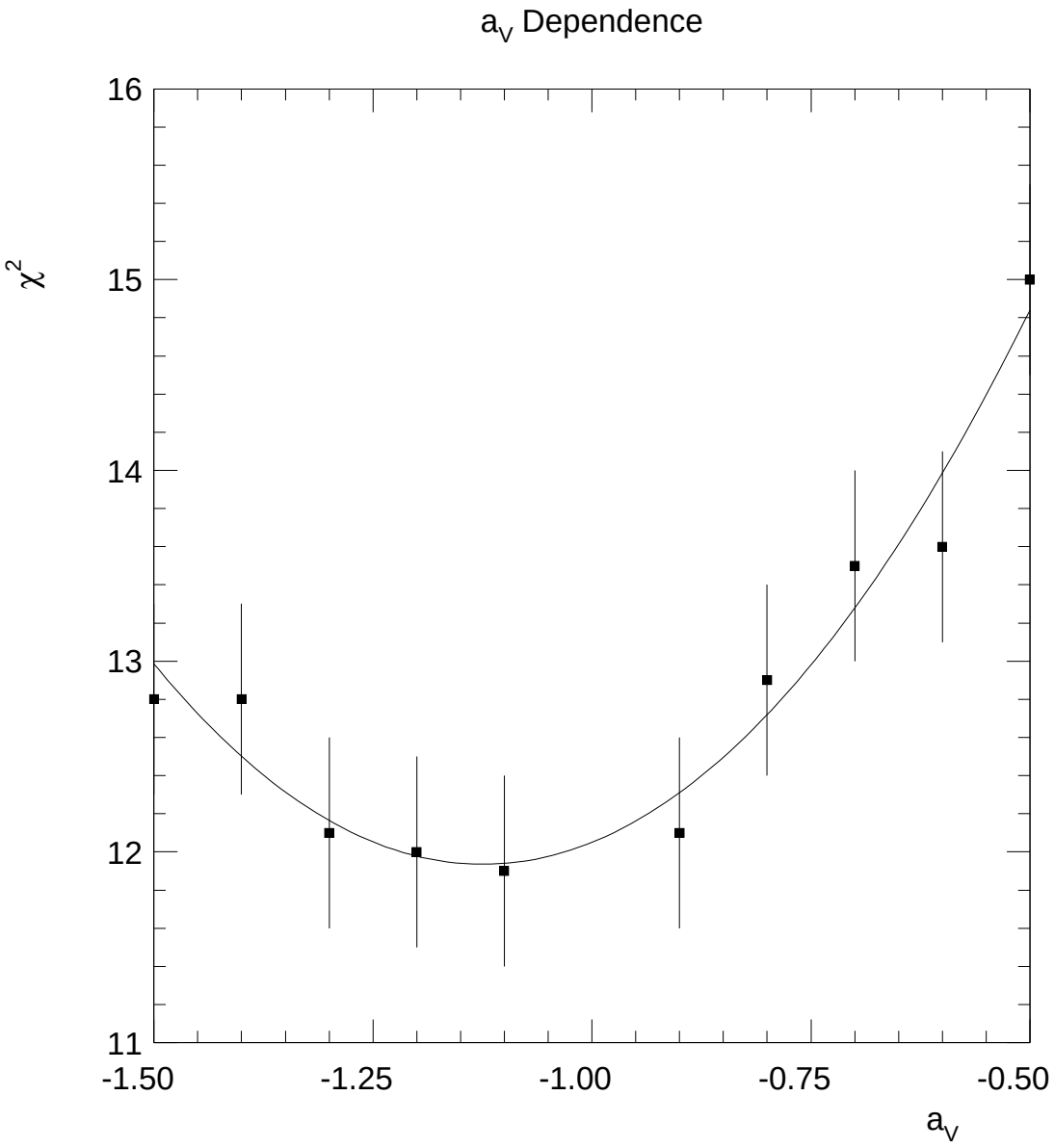

Figure 22: The χ^2 as a function of the value of a_V for the final data sample.

6 Conclusions

We have determined the branching ratio BR($K_L \rightarrow \pi^o e^+ e^- \gamma$) using the combined 1997 and 1999 data sets from KTeV. The statistics represents a factor of 2.5 over the previous 1997 result, consistent with the increased flux from the 1999 run. This analysis utilizes a number of new analysis techniques and has a somewhat improved understanding of the backgrounds. We find BR($K_L \rightarrow e^+ e^- \gamma$) = $(2.12 \pm 0.20 \pm 0.13) \times 10^{-8}$.

References

[1] J. Donoghue and F. Gabbiani, Phys. Rev. **D56**, 1605 (1997).

[2] A.Alabi-Harati et al., Phys. Rev. Lett. **87**, 021801 (2001).

[3] K. Murakami et al., Phys. Lett **B463** 333 (1999).

[4] G. Graham, Ph.D. Thesis, University of Chicago (1999).

Stage	Cut	Requirement
Crunch		
	2E-NCLUS	Require L3 tag bit
	Vertexing	Require vertex found
	Cluster/track match	Require all tracks match clusters
	E/p	$E/p > 0.9$
	HCC clusters	$N_{HCC} = 5$
	Vertex position	Vertex must be in beam.
	Five γ mass	$m_{5\gamma} > 0.380$
Analysis		
	Tracking	Two opposite signed tracks
	Clustering	Five hardware clusters
	Energy	$30 < ET < 210$
	Trigger counters	VV' verification
	Bad Spills (run$<$8245)	Reject Mask = 0x1072FFDF
	(run< 8577)	Reject Mask = 0x1073FFDF
	(run< 10000)	Reject Mask = 0x10727FDF
	(run> 10000)	Reject Mask = 0x10727FDB
	E/p	$0.95 < E/p < 1.05$
	Minimum Cluster Energy	$E_{min} > 2.0$
	x, y track separation	DC1 $x, y_{sep} > 0.01$
	π^o mass (best comb)	$0.130 < m_{\gamma\gamma} < 0.140$
	Decay vertex	$98 < z < 157$
	Collar Anti	$E_{CA} < 12$
	Beam hole cut	$d > 0.015$
	In-time pairs	No extra intime pairs
	Transverse momentum	$p_T > 0.003$
Background Reduction		
	Ring counters	$E_{RC} < 0.05$
	Spectrometer Antis	$E_{SA} < 0.1$
	$3\pi^o$ kinematics	$m_{\gamma\gamma\gamma}$ vs pp0kin cut
	Fusion χ^2 cut	FUSE3x3 < 4
	$2\pi^o$ kinematics	$NN > 0.95$
		$m_{e^+e^-\gamma} < 0.115$, $m_{e^+e^-\gamma} > 0.150$
	Track/Cluster distance	$d > 0.0125$
	Kaon mass	$0.490 < m_K < 0.505$

Table 1: List of all cuts used in this analysis.

	PRL result	1997 Data
Flux	2.80×10^{11}	2.87×10^{11}
Acceptance (%)	0.72	0.73
Signal Events	48	46
Background	3.6 ± 1.1	4.4 ± 1.49
Branching Ratio	2.21×10^{-8}	1.98×10^{-8}

Table 2: Values used in branching ratio calculation.

Systematic	1997 Data	1999 Data
a_V dependence	7.6	5.4
MC Statistics	4.2	3.7
FUSE3x3 cut	1.0	0.5
$3\pi^o$ z	1.0	1.3
$3\pi^o$ normalization	0.0	0.4
pp0kin cut	0.3	0.7
$3\pi^o$ p	0.3	0.4
$2\pi^o$ background	0.3	0.3
apertures	0.4	0.4
$2\pi^o$ z	0.2	0.2
p_T^2 cut	0.1	0.1
Total	8.8	6.8
K_L and π^o BR	2.8	

Table 3: Systematics in percent.